Mineralogical Magazine, October 2003, Vol. 67(5), pp. 831–853

A geochemical and Sr-Nd-O isotopic study of the Proterozoic Eriksfjord Basalts, Gardar Province, South Greenland: Reconstruction of an OIB signature in crustally contaminated rift-related basalts

R. HALAMA[1], T. WENZEL[1], B. G. J. UPTON[2], W. SIEBEL[1] AND G. MARKL[1,*]

[1] Universität Tübingen, Institut für Geowissenschaften, Wilhelmstr. 56, D-72074 Tübingen, Germany
[2] Department of Geology and Geophysics, The University of Edinburgh, West Mains Road, Edinburgh EH9 3JW, UK

ABSTRACT

Basalts from the volcano-sedimentary Eriksfjord Formation (Gardar Province, South Greenland) were erupted at around 1.2 Ga into rift-related graben structures. The basalts have compositions transitional between tholeiite and alkaline basalt with MgO contents <7 wt.% and they display *LREE*-enrichment relative to a chondritic source. Most of the trace element and *REE* characteristics are similar to those of basalts derived from OIB-like mantle sources. Initial $^{87}Sr/^{86}Sr$ ratios of clinopyroxene separates range from 0.70278 to 0.70383 and initial ε_{Nd} values vary from −3.2 to +2.1. The most unradiogenic samples overlap with the field defined by carbonatites of similar age and can be explained by mixing of isotopically depleted and enriched mantle components. Using AFC modelling equations, the Sr-Nd isotope data of the more radiogenic basalts can successfully be modelled by addition of <5% lower crustal granulite-facies gneisses as contaminants. $\delta^{18}O_{v\text{-}smow}$ values of separated clinopyroxene range from +5.2 to +6.0‰ and fall within the range of typical mantle-derived rocks. However, up to 10% mixing with an average lower crustal component are permitted by the data.

KEYWORDS: geochemistry, Sr-Nd-O isotopes, Gardar Province, basalt, Greenland.

Introduction

STUDY of rift-related basaltic magmatism is essential for an improvement in our understanding of the chemical composition of the sub-continental mantle and also the mechanisms responsible for the generation of flood basalts, alkaline rocks and carbonatites. It has been shown that several distinct mantle components can contribute to magmatism in rift-related environments (e.g. Perry *et al.*, 1987; Paces and Bell, 1989; Heaman and Machado, 1992), but that the relative importance of these sources is highly variable in both space and time (Shirey *et al.*, 1994, Nicholson *et al.*, 1997). For example, many occurrences of recent rift-related magmatism have a mantle-plume association (e.g. Baker *et al.*, 1997; Bell and Tilton, 2001). Studies of Proterozoic continental volcanic rocks provide insight into the composition of the mantle and the interplay between mantle and crustal magma sources at that time (e.g. Lightfoot *et al.*, 1991; Shirey *et al.*, 1994). In most models, three main mantle source components have been invoked to explain the geochemical signatures of the erupted rocks (1) Depleted MORB mantle (DMM), i.e. mantle sources of mid-ocean ridge basalts (MORBs) that are depleted in all incompatible elements. (2) OIB-like mantle, i.e. mantle known from ocean island basalts (OIBs), that is in oceanic regions restricted to islands that are not related to subduction (Hofmann, 1997). This type of mantle is less depleted or even enriched in

* E-mail: markl@uni-tuebingen.de
DOI: 10.1180/0026461036750147

incompatible elements compared to the primitive mantle. There are several types of OIB components well defined by Sr-Nd-Pb isotopic studies (Zindler and Hart, 1986; Hart *et al*., 1992). These are HIMU ('high μ', $\mu \equiv {}^{238}U/{}^{206}Pb$), enriched mantle 1 (EM-1) and enriched mantle 2 (EM-2). (3) Subcontinental lithospheric mantle (SCLM), representing the mantle below the continental crust. The SCLM is usually enriched in incompatible elements, but it can be very heterogeneous.

Interaction of an OIB-like source with lithospheric mantle (Ormerod *et al*., 1988; Paslick *et al*., 1995; Molzahn *et al*., 1996) or DMM (e.g. Nicholson *et al*., 1997) may have played a major role in magma genesis of continental volcanic rocks. Lavas chemically similar to OIBs have been observed in many continental flood basalt provinces, e.g. Deccan Traps (Mahoney, 1988), British Tertiary Volcanic Province (Fitton *et al*., 1997) and Paraná-Etendeka (Gibson *et al*., 1997). These are believed to represent mantle-derived melts from plumes not contaminated by lithospheric material, but they represent only a small proportion of the total magma volume erupted (Gibson *et al*., 1999). Therefore, the SCLM has been invoked in various models either as a source of large-scale melts (e.g. Turner *et al*., 1996) or as assimilant in plume-derived melts (e.g. Gibson *et al*., 1995). The SCLM appears to be especially important in the genesis of small-degree melts (Gibson *et al*., 1999). Post-Archaean lithospheric mantle is considered to have been sufficiently fertile to have contributed to the genesis of flood basalts (Hawkesworth *et al*., 1990).

The Gardar Province in South Greenland is a rift-related igneous province with magmatism lasting from about 1.35 to 1.14 Ga (Emeleus and Upton, 1976; Upton and Emeleus, 1987; Upton *et al*., 2003). It comprises about 12 main igneous complexes, numerous dykes of variable chemical composition, and a sequence of rift-related interlayered lavas and sediments (Eriksfjord Formation). The basaltic lavas of the Eriksfjord Formation are among the geochemically most primitive rocks of the Province. However, except for detailed palaeomagnetic investigations (Thomas and Piper, 1992; Piper *et al*., 1999), they have been studied relatively little (Larsen, 1977; Paslick *et al*., 1993). Due to their comparatively primitive nature, the basaltic rocks of the Eriksfjord Formation provide a good opportunity to discern the geochemical signatures of the mantle sources of the magmatic activity of the Province. Similar sources may have been involved in the petrogenesis of the Gardar anorthosites, alkali gabbros and nepheline syenites. In this study, we present new geochemical data (XRF analyses of major and trace elements, Sr, Nd and O isotopic analyses, *REE* analyses of whole-rock samples and *in situ REE* analyses of clinopyroxene) to constrain mantle sources and to determine the role of crustal contamination in the petrogenesis of the Eriksfjord Formation basalts. In particular, high-precision laser-fluorination oxygen isotope data have only recently become an important tool for evaluating the contribution of mantle and continental crust in suites of continental flood basalts (Baker *et al*., 2000). Since continental intraplate basalts are the only major class of terrestrial basalts that have not yet been explored systematically using these methods (Eiler, 2001), the laser fluorination oxygen isotope data of clinopyroxene separates presented herein are an important contribution to the knowledge of oxygen isotopic compositions of continental basalts in general.

Geological setting

The Eriksfjord Formation (EF) represents an ~3500 m thick sequence of Precambrian supracrustal rocks comprising continental sandstones and conglomerates and eruptive rocks and sills that range from basalt through trachyte to alkaline phonolite and carbonatite (Larsen, 1977). The rocks lie unconformably on the Ketilidian Julianehåb batholith dated at 1.85 to 1.79 Ga (van Breemen *et al*., 1974; Garde *et al*., 2002) and are cut by the 1.16 Ga Ilímaussaq intrusion (Waight *et al*., 2002). The type-section of the Eriksfjord Formation occurs on the Ilímaussaq peninsula, and has been subdivided into six stratigraphic groups (Thomas and Piper, 1992), originally defined as members (Poulsen, 1964) (Fig. 1). The three volcanic groups are known as, from oldest to youngest, Mussartût, Ulukasik and Ilímaussaq. The Mussartût Group is subdivided into nine sub-units and the Ilímaussaq Group is subdivided into three sub-units, called Sermilik, Tunugdliarfik and Narssaq Fjeld (Fig. 1). A sandstone unit precedes each volcanic group (Thomas and Piper, 1992). The Mussartût Group contains the Qassiarsuk carbonatite complex, dated at ~1.2 Ga by Rb-Sr and Pb-Pb isochrons (Andersen, 1997). Paslick *et al.* (1993) obtained two Sm-Nd isochron ages of 1.17±0.03 and

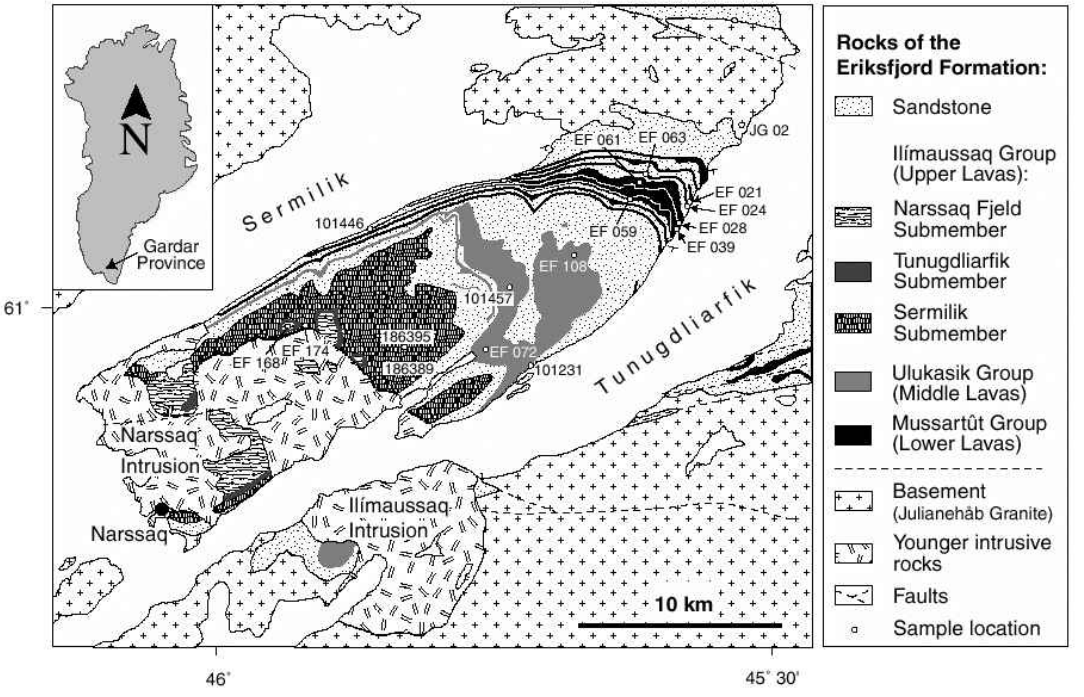

FIG. 1. Map of the Eriksfjord Formation on the Narssaq peninsula with sample locations (after Poulsen, 1964 and Larsen, 1977). Sample 101472 (not shown) is from a succession ~2 km south of the settlement of Narsarsuaq further to the NE.

1.20±0.03 Ga for two samples of the Ulukasik Group. However, palaeomagnetic data indicate an age of 1.35–1.31 Ga for the entire succession (Piper *et al.*, 1999) and the exact age of the EF is as yet unresolved (Upton *et al.*, 2003). Parts of the Eriksfjord lavas have been subjected to extensive metasomatism related to the intrusion of alkaline magmas (Ranlov and Dymek, 1991; Coulson and Chambers, 1996). The local presence of epidote implies thermal metamorphism at temperatures of up to 300–350ºC (Piper *et al.*, 1999). High eruption rates are inferred for the volcanic system and the whole lifespan is considered to be <~5 Ma (Piper *et al.*, 1999).

Analytical procedures

Electron microprobe analysis

Mineral compositions were determined using a JEOL 8900 electron microprobe (EMP) at the Institut für Geowissenschaften, Universität Tübingen, Germany. An internal φρz correction of the raw data was applied (Armstrong, 1991). Both natural and synthetic standards were used for major and minor elements. Measuring times were 16 s and 30 s on the peak positions for major and minor elements, respectively. The emission current was 15 nA and the acceleration voltage 15 kV. For feldspar analyses, a beam diameter of 5 μm was used to avoid errors resulting from diffusion of Na.

XRF analysis

Whole-rock analyses were performed by standard X-ray fluorescence (XRF) techniques at the Institut für Geowissenschaften at the Johannes Gutenberg-Universität Mainz, Germany, using a Philips PW 1404 spectrometer, and at the Universität Freiburg, using a Philips PW 2404 spectrometer. Prior to analysis, whole-rock samples were crushed and milled in tungsten carbide mills. The powders obtained were dried at 105ºC. Loss on ignition (LOI) determinations were carried out on 1 g of pulverized sample material which was heated for 2 h at 1000ºC. Pressed powder pellets and fused glass discs were prepared to measure contents of trace and major elements, respectively. Natural standards were used for calibration. Detection limits vary

between 1 and 9 ppm, depending on the specific trace element and on the instrument used.

Whole-rock REE analyses

Whole-rock *REE* analyses were carried out by the Natural Environment Research Council (NERC) inductively coupled plasma-atomic emission spectrometry (ICP-AES) facility at Royal Holloway, University of London. Solutions were prepared using a combined HF dissolution and alkali fusion as described in Walsh *et al.* (1981). Resultant solutions were analysed for 12 *REE*s and selected potential interferences using a Perkin Elmer Optima 3300RL ICP-AES.

Laser ICP-MS in situ REE measurement of clinopyroxene

In situ laser ablation inductively coupled plasma-mass spectrometer (LA-ICP-MS) *REE* analyses on ~150 μm thick polished thin sections were performed at the EU Large-Scale Geochemical Facility (University of Bristol) using a VG Elemental PlasmaQuad 3 + S-Option ICP-MS equipped with a 266 nm Nd-YAG laser (VG MicroProbe II). The laser beam diameter at the sample surface was ~20 μm. All measurements were made using Thermo Elemental PlasmaLab 'time-resolved analysis' (TRA) data acquisition software with a total acquisition time of 100 s per analysis, allowing ~40 s for background followed by 50 s for laser ablation. NIST 610 glass was used for instrument calibration, and NIST 612 was used as a secondary standard. Ca was used as an internal standard to correct the ablation yield differences between and during individual analyses on both standards and samples. To avoid analytical uncertainties due to variations in the concentrations of the internal standard, Ca concentrations were quantitatively measured within 20 μm of the laser ablation pits using the EMP at the Institut für Geowissenschaften, Universität Tübingen. The precision of trace-element concentrations, based on repeated analyses of standards, is ~±5% for element concentrations >10 ppm and ±10% for concentrations <10 ppm. Data processing was carried out offline using the same PlasmaLab software used for data collection and various custom-designed Excel spreadsheets. The limits of detection are defined as 3.28 standard deviations above background level, which is equal to a 95% confidence that the measured signal is significantly above background. Typical detection limits for the *REE* in this study were 0.04–0.6 ppm.

Sr and Nd isotope analysis

For Sr and Nd isotope analyses, 15–20 mg samples of hand-picked clinopyroxene were spiked with mixed ^{84}Sr–^{87}Rb and ^{150}Nd–^{149}Sm tracers before dissolution under high pressure in HF at 180°C in poly-tetrafluor-ethylene (PTFE) reaction bombs. The Rb and Sr were separated in quartz columns containing a 5 ml resin bed of AG50W-X12, 200–400 mesh, equilibrated with 2.5 N HCl. The Sm and Nd separation was performed in quartz columns, using 1.7 ml Teflon powder coated with HDEHP (Di-Ethyl Hexyl Phosphate) as the cation exchange medium, equilibrated with 0.18 N HCl. All analyses were made with a multicollector Finnigan MAT 262 thermal ionization mass spectrometer (TIMS) in static collection mode at the Institut für Geowissenschaften, Universität Tübingen. The Sr was loaded with a Ta-HF activator and measured on a single W filament. The Rb, Sm and Nd were measured in a double Re-filament configuration mode. $^{87}Sr/^{86}Sr$ and $^{143}Nd/^{144}Nd$ ratios were normalized for mass fractionation to $^{86}Sr/^{88}Sr = 0.1194$ and $^{146}Nd/^{144}Nd = 0.7219$, respectively. The average $^{143}Nd/^{144}Nd$ ratio obtained for the Ames Nd-standard (Geological Survey of Canada, Roddick *et al.*, 1992) was 0.512119±10 ($n = 42$) and the average $^{87}Sr/^{86}Sr$ ratio for the NBS 987 Sr-standard was 0.710261±16 ($n = 30$) during the course of this study. $^{143}Nd/^{144}Nd$ ratios have been cross-checked with the La Jolla Nd-standard which gave 0.511831±30 ($n = 12$). Total procedural blanks (chemistry and loading) were <200 pg for Sr and <100 pg for Nd.

Oxygen isotope analysis

The oxygen isotope composition of hand-picked clinopyroxene separates was measured using a method similar to that described by Sharp (1990) and Rumble and Hoering (1994). 1–2 mg of hand-picked clinopyroxene were loaded onto a Pt-sample holder. The sample chamber was pumped out to a vacuum of $\sim 10^{-6}$ mbar and pre-fluorinated overnight. Samples were then heated with a CO_2-laser in an atmosphere of 50 mbar of pure F_2. Excess F_2 is separated from O_2 by conversion to Cl_2 using KCl held at 150°C. The extracted O_2 is collected on a molecular sieve (13X). Oxygen isotopic compositions were measured on a Finnigan MAT 252 mass spectrometer at the Institut für Geowissenschaften, Universität Tübingen. The results are reported as

the per mil deviation from Vienna Standard Mean Ocean Water (V-SMOW) in the standard δ-notation. Replicate oxygen isotope analyses of the NBS-28 quartz standard (Valley *et al.*, 1995) had an average precision of ±0.1‰ for $\delta^{18}O$. In each run, standards were analysed at the beginning and the end of the sample set. A correction was applied to the data equal to the average of the difference between the mean measured value and the accepted value for the standard (9.64‰).

Oxygen isotope compositions of powdered whole-rock samples were determined by a conventional method modified after Clayton and Mayeda (1963), using BrF_5 as reagent and converting the liberated oxygen to CO_2 before mass spectrometric analysis.

Petrography

175 samples were collected from all three volcanic units of the Eriksfjord Formation, but most of them were extensively altered. They contained secondary chlorite, Fe-talc, Ca-Fe silicates and carbonate as alteration products. Since the focus of this study was *in situ* analyses of minerals or analyses of mineral separates, only nine samples with a significant proportion of fresh clinopyroxene and relatively few alteration products were selected for analysis. Due to the limited number of suitable samples, we did not attempt to investigate the lavas in terms of their stratigraphic position. In addition to the nine samples from which pyroxene separates were obtained, *REE* whole-rock data of six other samples were added to the data set.

In general, the Mussartût Group lavas are olivine-free, but contain up to 50% chloritic matrix that probably results from devitrification of former glass. In contrast, the majority of Ulukasik and Ilímaussaq Group lavas contain olivine-pseudomorphs and tend to be coarser grained and holocrystalline. Many of them contain 'snow-flake' glomerocrysts of plagioclase indicating plagioclase-saturation or super-saturation at near-surface levels (Upton, 1996). The samples from which clinopyroxenes have been separated are fine-grained basalts with plagioclase laths embedded in interstitial clinopyroxene as the major and apatite and Fe-Ti oxides as subordinate primary magmatic mineral phases. The texture can be described as ophitic and is believed to result from the cotectic crystallization of plagioclase and clinopyroxene (Philpotts, 1990). Olivine has been present in a few samples, but it is now completely altered. Pyrite, pyrrhotite and chalcopyrite occur as accessory phases. Some samples contain two oxides (ilmenite + titanomagnetite), whereas others contain a single oxide exsolved into ilmenite and titanomagnetite or ilmenite and hematite. Texturally, they are mostly subhedral to anhedral, although few euhedral grains occur. Hematite is also present around both discrete and exsolved ilmenite and titanomagnetite grains and the exsolved hematite might be entirely of secondary origin formed by oxidation of titanomagnetite. Late-stage interstitial quartz occurs rarely. Sample EF 108 (Ulukasik Group) is remarkable in having an intense reddish colour unlike the other samples that are almost black.

Results

Mineral chemistry

Typical analyses of clinopyroxenes are given in Table 1. Compositions range from $En_{41}Wo_{44}Fs_{16}$ to $En_{28}Wo_{45}Fs_{27}$ and broadly overlap for all groups (Fig. 2). According to the classification of Morimoto *et al.* (1988), clinopyroxenes of the Mussartût and Ulukasik Groups are mainly augites with few diopsides present, whereas in the Ilímaussaq Group samples of diopsidic compositions dominate over augitic ones. Clinopyroxene analyses from the various samples form tight clusters on the pyroxene quadrilateral except for those from sample EF 108 that are more scattered. With only a single pyroxene phase present in all samples, clinopyroxene compositions indicate minimum crystallization temperatures (Lindsley, 1983) of 750–1000ºC (Fig. 2). Plagioclase is normally zoned and its composition typically varies between $An_{70}Ab_{29}Or_1$ and $An_{16}Ab_{72}Or_{12}$. Late interstitial albite can reach compositions of $An_0Ab_{99}Or_1$. There are no significant composi-

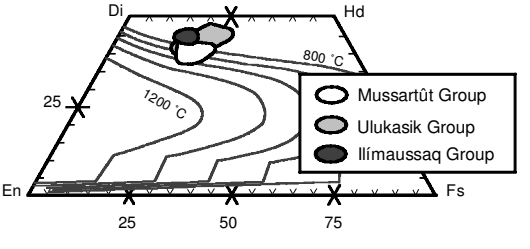

FIG. 2. Clinopyroxene analyses of the Eriksfjord basalts plotted in the pyroxene quadrilateral with isotherms after Lindsley (1983).

TABLE 1. Typical clinopyroxene analyses of Eriksfjord Formation basalts determined by EMP.

Sample	EF 024	EF 024	EF 039	EF 059	EF 072	EF 108	EF 168	EF 174
Cpx no.	cpx 2	cpx 3	cpx 5	cpx 3	cpx 5	cpx 7	cpx 4	cpx 1
SiO_2	50.60	50.41	51.28	49.88	51.45	49.50	51.75	50.69
TiO_2	1.73	1.76	1.21	1.69	1.40	1.62	0.96	1.21
Al_2O_3	2.97	3.00	1.79	2.23	1.71	2.64	1.55	2.13
FeO	11.60	10.68	12.18	14.05	9.93	12.34	9.79	11.29
MnO	0.28	0.21	0.30	0.40	0.19	0.28	0.25	0.31
MgO	12.54	13.24	12.63	11.82	13.25	11.63	13.07	12.14
CaO	19.59	20.29	20.02	19.07	21.06	20.99	21.74	21.43
Na_2O	0.34	0.31	0.29	0.49	0.33	0.55	0.52	0.54
Total	99.65	99.89	99.71	99.63	99.32	99.55	99.62	99.74
Formulae based on 4 cations and 6 oxygens:								
Si	1.91	1.89	1.94	1.90	1.94	1.88	1.94	1.91
Al	0.13	0.13	0.08	0.10	0.08	0.12	0.07	0.09
Ti	0.05	0.05	0.03	0.05	0.04	0.05	0.03	0.03
Fe^{3+}	-	-	-	0.03	-	0.07	0.03	0.05
Mg	0.71	0.74	0.71	0.67	0.75	0.66	0.73	0.68
Fe^{2+}	0.37	0.33	0.39	0.41	0.31	0.32	0.28	0.31
Mn	0.01	0.01	0.01	0.01	0.01	0.01	0.01	0.01
Ca	0.79	0.82	0.81	0.78	0.85	0.85	0.87	0.87
Na	0.02	0.02	0.02	0.04	0.02	0.04	0.04	0.04
Total	4.00	4.00	4.00	4.00	4.00	4.00	4.00	4.00
Pyroxene projection after Lindsley (1983):								
Wo	0.39	0.41	0.41	0.41	0.43	0.43	0.45	0.44
En	0.40	0.41	0.39	0.37	0.40	0.38	0.40	0.38
Fs	0.21	0.18	0.21	0.23	0.17	0.19	0.15	0.17

tional changes among the various samples. Ilmenite from two samples (EF 024 and EF 039) which contain coexisting ilmenite and titanomagnetite includes a significant component of pyrophanite ($MnTiO_3$) with up to 8.7 wt.% MnO. Its compositions vary between $Ilm_{86}Hem_5Pyr_8$ and $Ilm_{76}Hem_5Pyr_{19}$. Titanomagnetite analyses were unsatisfactory as all grains show strong alteration. They are considered unreliable and are not presented here.

Whole-rock geochemistry and classification

Concentrations of major and trace elements are summarized in Table 2. The basalts can be classified according to the TAS diagram (Le Maitre *et al.*, 1989) as basalts and trachybasalts with both alkaline and subalkaline compositions (not shown). Due to possible mobility of the Na and K, the samples were also plotted into Nb/Y *vs.* Zr/P_2O_5 and P_2O_5 *vs.* Zr diagrams (Floyd and Winchester, 1975) which can discriminate between tholeiitic and alkaline series. These diagrams do not yield consistent discriminations for the EF basalts, but indicate that the character of the sample suite is transitional between tholeiitic and alkaline (not shown).

Mg# [$100Mg/(Mg+Fe^{2+})$], calculated assuming $Fe_2O_3/FeO = 0.2$ as recommended for basalts by Middlemost (1989), varies between 54 and 40 (Table 2). Ni concentrations range from 46 to 115 ppm and Cr contents from 29 to 126 ppm. Taking Mg# as fractionation index, a positive correlation ($r^2 = 0.61$) with Ni contents indicates fractionation of olivine (Fig. 3). The relatively poor positive correlations of Mg# with Cr ($r^2 = 0.44$) and Sc ($r^2 = 0.23$) argue against a significant fractionation of Cr-spinel or clinopyroxene. This is consistent with the lack of clinopyroxene phenocrysts and the absence of any Cr-spinel. The negative correlations of Mg# with Sr, TiO_2 and P_2O_5 suggest that fractionation of plagioclase, Fe-Ti oxides and apatite was not important in the sample set investigated, which is again consistent

TABLE 2. XRF whole-rock analyses of Eriksfjord Formation basalts.

Sample	EF 024	EF 063	EF 061	EF 039	EF 059	EF 108	EF 072	EF 174	EF 168
Group	Mussartût	Mussartût	Mussartût	Mussartût	Mussartût	Ulukasik	Ulukasik	Ilímaussaq	Ilímaussaq
Subunit	4	4	5	6	7	Lower Unit	Upper Unit	Sermilik	Narssaq Fjeld
Major elements (wt.%)									
SiO_2	45.73	45.85	46.88	46.60	48.75	46.98	46.56	46.01	45.45
TiO_2	2.30	2.00	1.80	1.75	1.91	2.65	2.03	2.99	2.77
Al_2O_3	15.78	16.30	16.00	16.12	16.45	16.82	16.68	16.45	17.19
Fe_2O_3	15.10	13.56	13.31	13.83	12.25	13.94	13.21	14.38	13.92
MnO	0.28	0.18	0.18	0.18	0.17	0.14	0.17	0.18	0.17
MgO	5.25	6.83	6.53	6.73	5.68	3.96	6.47	4.40	4.80
CaO	8.42	8.49	8.72	8.57	9.20	6.41	8.08	7.46	7.37
Na_2O	3.49	2.74	2.89	2.76	2.36	4.48	3.03	3.23	3.76
K_2O	0.87	0.83	0.68	0.32	0.27	1.59	0.70	2.05	1.32
P_2O_5	0.41	0.35	0.23	0.23	0.23	0.48	0.35	1.11	0.83
LOI	1.99	2.10	2.40	2.38	2.42	2.04	2.10	0.52	1.56
Total	99.62	99.23	99.62	99.47	99.69	99.49	99.38	98.78	99.14
Mg#	45.3	54.5	53.8	53.6	52.4	40.3	53.8	42.1	45.0
Trace elements (ppm)									
Sc	24	22	25	22	26	19	20	21	16
V	209	175	215	195	211	142	170	164	203
Cr	81	108	66	65	126	48	82	33	29
Co	63	78	70	62	71	44	68	35	46
Ni	99	115	85	85	101	58	106	46	51
Cu	65	49	46	60	97	41	59	38	41
Zn	103	102	110	97	110	93	82	122	105
Ga	20	18	21	19	20	19	16	21	19
Rb	24	26	16	< 10	< 10	38	12	39	45
Sr	504	503	512	392	373	712	507	850	992
Y	31	26	28	23	28	31	17	31	25
Zr	188	165	121	116	125	125	88	164	139
Nb	12	11	10	< 10	10	9	< 10	31	27
Ba	445	375	415	302	178	582	405	1293	900
Pb	6	7	3	4	3	4	4	3	5
La	–	–	15	–	12	11	–	37	28
Ce	–	–	40	–	38	39	–	92	71
Pr	–	–	1	–	1	2	–	9	4
Nd	–	–	16	–	15	18	–	43	34
Sm	–	–	6	–	7	6	–	5	5
CIPW norm:									
q	–	–	–	–	3.13	–	–	–	–
or	5.14	4.91	4.02	1.89	1.60	9.40	4.14	12.12	7.80
ab	28.07	23.19	24.45	23.35	19.97	32.07	25.64	27.33	29.81
an	24.82	29.73	28.68	30.65	33.50	21.09	29.85	24.33	26.13
ne	0.79	–	–	–	–	3.16	–	–	1.09
di	11.87	8.30	10.76	8.53	8.77	6.33	6.54	4.52	4.16
hy	–	8.90	10.59	16.50	22.17	–	10.97	3.15	–
ol	16.70	13.09	10.44	7.80	–	14.72	11.20	13.88	16.89
mt	3.65	3.28	3.22	3.35	2.96	3.36	3.19	3.48	3.36
il	4.37	3.80	3.42	3.32	3.63	5.03	3.86	5.68	5.26
ap	0.95	0.81	0.53	0.53	0.53	1.11	0.81	2.57	1.92

Mg# was calculated as Mg# = $100*Mg^{2+}/(Mg^{2+}+Fe^{2+})$ using $Fe_2O_3/FeO = 0.2$. Normative mineral compositions were determined according to the CIPW calculation scheme.

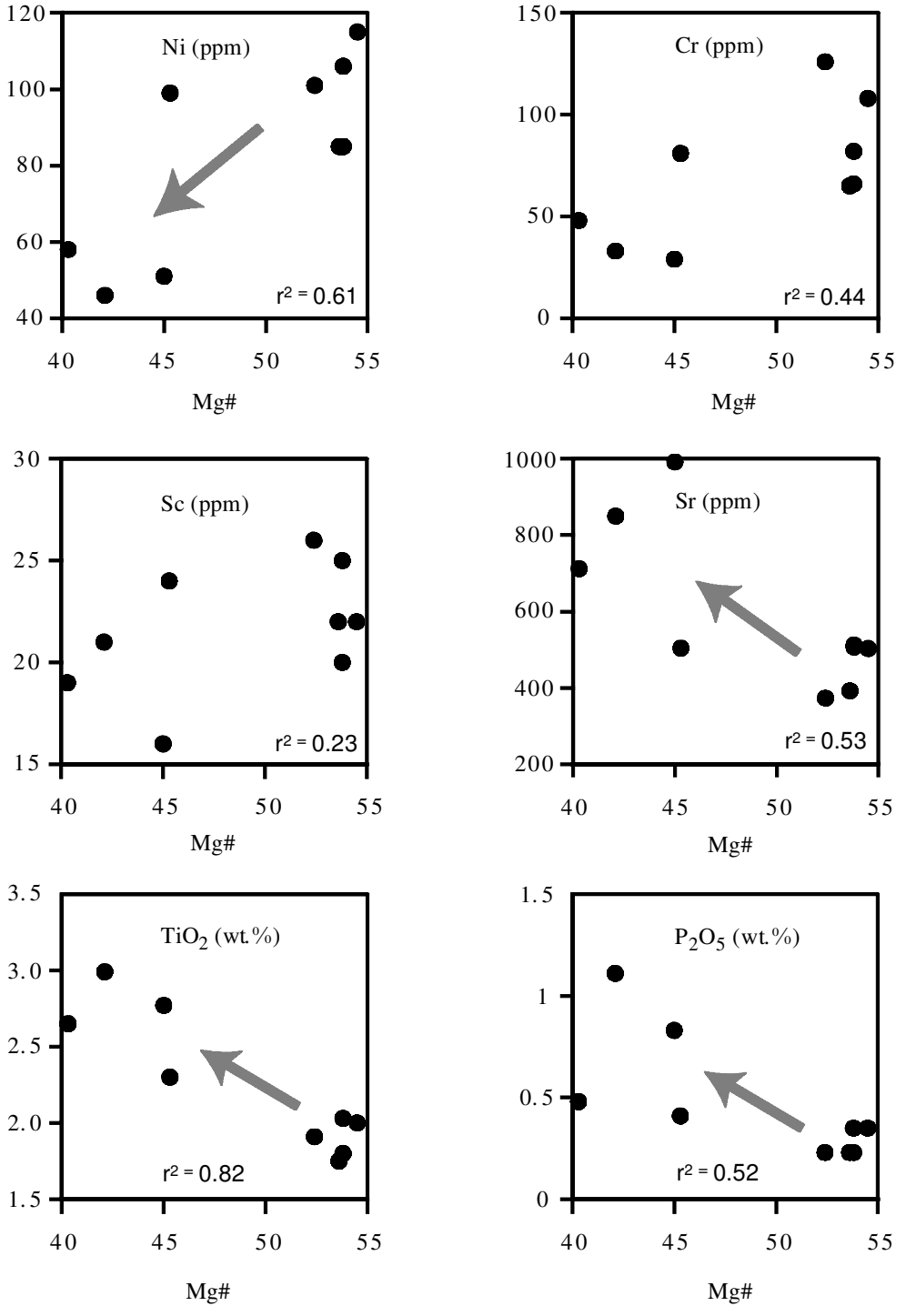

FIG. 3. Whole-rock variation diagrams for EF basalts with Mg# as fractionation index. Mg# is calculated as $Mg/(Mg+Fe^{2+})$ with $Fe_2O_3/FeO = 0.2$ (Middlemost, 1989).

with the mostly subhedral Fe-Ti oxides and the ophitic texture. Ratios of incompatible trace elements, such as Zr/Y (range: 4.0–6.3) and Ti/Y (range: 385–716), are relatively uniform throughout all samples, but some scatter is evident. Notable geochemical features are high Sr contents up to 1000 ppm and very high Ba contents up to 1300 ppm.

Normative mineral compositions were determined according to the CIPW calculation scheme (Cross *et al.*, 1903; Cox *et al.*, 1979). Most samples are hypersthene-normative, some are nepheline-normative and one (EF 059) is quartz-normative (Table 2). Despite the uncertainties involved in the CIPW norm calculation, the data indicate that some of the basalts crystallized from silica-undersaturated magmas and others from distinct silica-saturated or -oversaturated magmas.

Multi-element diagrams normalized to primitive mantle values show that the EF basalts are enriched in all incompatible elements relative to primitive mantle values (Fig. 4). The patterns of the EF basalts are characterized by a prominent Ba peak, a subordinate P peak and a decreasing element enrichment with increasing compatibility. In comparison with normal MORB (N-MORB), enriched MORB (E-MORB) and average OIB (Sun and McDonough, 1989), the patterns of the EF basalts are closest to those of OIB both in shape and normalized concentrations.

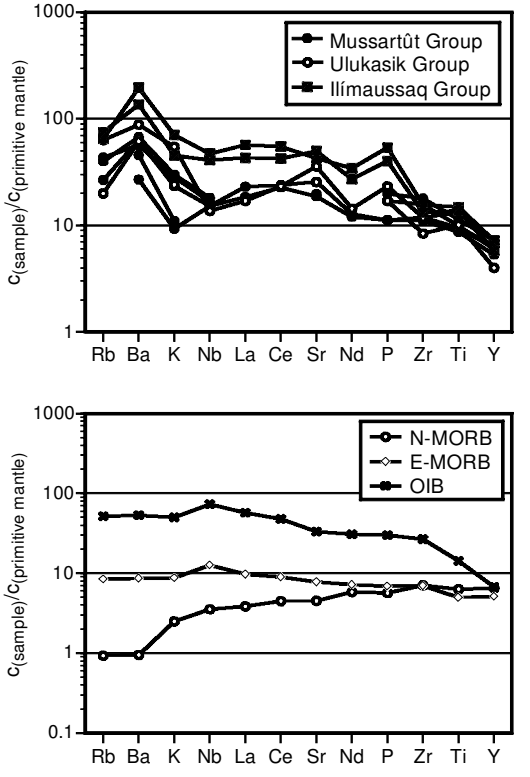

FIG. 4. Multi-element plots normalized to primitive mantle values (McDonough and Sun, 1995). Data for N-MORB, E-MORB and average OIB (Sun and McDonough, 1989) are shown for comparison.

Whole-rock REE data

Whole-rock *REE* data are presented in Table 3 and *REE* concentrations, normalized to chondritic values of Boynton (1984), are shown in Fig. 5*a*. All samples are characterized by *LREE*-enriched patterns with no, or slightly positive, Eu anomalies (Eu/Eu* = 0.97 to 1.13). La concentrations are roughly 20–60 times and Lu concentrations are 10 times chondritic values. Normalized *LREE* abundances from La to Nd are fairly constant, but the patterns show a steady and smooth decline from Nd towards heavier *REE*. The *REE* patterns of the EF basalts fall in between those of typical OIB and E-MORB (Fig. 5*b*). They have similar patterns and absolute abundances compared to basaltic dykes from the Ivittuut area, South Greenland (Goodenough *et al.*, 2002). La_N/Sm_N, as a measure of *LREE* fractionation, has a restricted range from 1.30 to 1.65. The degree of HREE fractionation expressed as Gd_N/Yb_N is slightly more variable and ranges from 1.57 to 2.57. Both these ratios of the EF basalts fall generally between typical OIB and E-MORB compositions.

Clinopyroxene REE patterns

Typical analyses of *REE* concentrations in clinopyroxenes are given in Table 3. They show that *REE* concentrations in individual minerals of one particular sample can be quite variable. Chondrite-normalized *REE* patterns of clinopyroxenes are very similar in the samples from the Mussartût and Ulukasik Groups (Fig. 6*a,b*). They are enriched in all *REE* relative to chondritic values and the patterns show a fairly steep increase from La to Sm, followed by a gradual, smooth decrease from Sm to Lu. Clinopyroxenes from sample EF 168 (Ilímaussaq Group) are distinct as they have generally higher *REE* contents, especially in the *LREE*, and a weak Eu anomaly (Fig. 6*c*). The 3–10× enrichment in Nd

TABLE 3. *REE* data of whole rocks and clinopyroxenes, the latter determined by Laser ICP-MS.

	Whole-rock analyses:						Representative clinopyroxene analyses:							
Sample no.	101231	101446	101457	101472	186389	186395	EF 024-2	EF 039-1	EF 039-2	EF 039-4	EF 072-2	EF 072-3	EF 168-3	EF 168-5
REE concentrations (ppm)														
La	11.65	18.06	10.29	6.61	15.54	12.28	4.40	2.66	1.99	1.50	2.73	3.04	16.55	27.59
Ce	29.03	46.05	24.96	17.13	37.81	30.08	18.04	11.46	8.68	7.17	10.50	12.60	57.23	99.67
Pr	4.34	6.7	3.88	2.68	5.27	4.33	3.31	2.16	1.81	1.28	2.49	2.62	10.29	17.43
Nd	20.06	31.71	17.64	12.49	25.09	20.16	19.02	13.82	12.22	8.98	15.64	15.72	58.51	96.06
Sm	4.75	6.97	4.04	3.21	5.91	4.82	6.66	4.19	4.28	3.27	6.07	7.06	15.82	26.59
Eu	1.74	2.5	1.57	1.07	1.97	1.72	1.83	1.49	1.11	1.21	2.00	1.94	3.87	7.07
Gd	4.82	6.58	4.04	3.55	5.8	4.99	6.96	5.61	5.24	4.32	6.15	6.05	14.75	25.27
Tb	–	–	–	–	–	–	1.35	1.01	0.77	0.71	1.11	1.21	2.31	3.61
Dy	4.47	5.22	3.61	3.56	5.35	4.81	6.86	5.93	4.78	4.25	5.99	6.86	13.10	20.52
Ho	0.92	1.04	0.73	0.73	1.1	1.01	1.48	1.40	1.00	1.00	1.21	1.29	2.39	4.24
Er	2.43	2.53	1.95	1.97	2.87	2.66	3.89	3.34	2.64	2.11	2.99	3.64	6.53	9.60
Tm	–	–	–	–	–	–	0.45	0.39	0.36	0.29	0.35	0.44	0.86	1.27
Yb	2.18	2.07	1.74	1.83	2.59	2.36	3.78	2.81	2.49	2.45	2.70	3.01	6.78	8.89
Lu	0.34	0.31	0.26	0.27	0.39	0.35	0.46	0.41	0.30	0.31	0.52	0.41	1.25	1.60
$(Eu/Eu^*)_N$	1.11	1.13	1.19	0.97	1.03	1.07	0.82	0.94	0.72	0.99	1.00	0.91	0.77	0.83

Eu anomaly is calculated as $(Eu/Eu^*)_N = Eu_N/(Sm_N \times Gd_N)^{0.5}$, normalized to chondrite values from Boynton (1984).

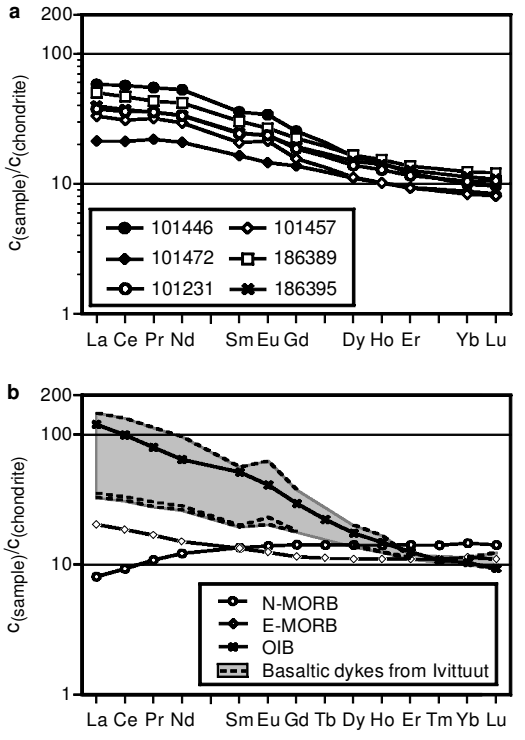

FIG. 5. (*a*) Whole-rock *REE* data of EF basalts, normalized to chondritic values from Boynton (1984). (*b*) Typical compositions of N-MORB, E-MORB and OIB (Sun and McDonough, 1989) are shown for comparison.

in clinopyroxenes of EF 168 compared to the other samples (EF 024, 039 and 072) seems only partly due to a higher degree of fractionation since the Mg# value of EF 168 is only slightly lower. Thus, the *LREE* enrichment appears to underline the more alkaline character of this sample. A comparison with published *REE* patterns of clinopyroxenes (Fig. 6*d*) shows that the EF patterns are unlike patterns from olivine gabbros with MORB-like signatures (Benoit *et al.*, 1996), but fairly similar to clinopyroxene megacryst patterns from an OIB-like alkaline basalt (Nimis and Vannucci, 1995).

Sr, Nd and O isotopic composition

Sr, Nd and O isotopic compositions of all samples are presented in Table 4. Sr and Nd isotopic compositions of the clinopyroxene separates have been recalculated to an approximate eruption age of 1.2 Ga (Paslick *et al.*, 1993) using decay constants of 1.42×10^{-11} a^{-1} for ^{87}Rb (Steiger and Jäger, 1977) and 6.54×10^{-12} a^{-1} for ^{147}Sm (Lugmair and Marti, 1978). Present day CHUR values of 0.1967 for ^{147}Sm/^{144}Nd (Jacobsen and Wasserburg, 1980) and 0.512638 for ^{143}Nd/^{144}Nd (Goldstein *et al.*, 1984) were used to calculate initial ε_{Nd} values. ^{87}Sr/^{86}Sr initial ratios are fairly constant and range from 0.70278 to 0.70383 (Table 4). ε_{Nd}(i) values vary from −3.2 to +2.1 (Table 4). On the Sr-Nd isotope diagram, the EF basalts define a relatively steep trend (Fig. 7) with initial ^{87}Sr/^{86}Sr ratios similar to those of the Bulk Silicate Earth (BSE). Only one sample is slightly displaced towards a more radiogenic initial ^{87}Sr/^{86}Sr ratio. None of the samples has an ε_{Nd} value close to depleted mantle values, estimated to be between ε_{Nd} = +5.3 (calculated after DePaolo, 1981) and ε_{Nd} = +7.3 (calculated after Goldstein *et al.*, 1984) at 1.2 Ga. The two alkaline basalts of the Ilímaussaq Group are within the range of the other data, but they define a restricted field around CHUR and BSE, respectively. Errors induced by the uncertainty in the age of the EF basalts are largely within the error of the isotope analyses and do not change the overall picture. In comparison with other published Sr-Nd isotope data from the Gardar Province, the initial Sr isotope ratios of the EF basalts are very similar to relatively primitive basaltic, lamprophyric and carbonatitic dyke rocks which have $(^{87}Sr/^{86}Sr)_i$ of ~0.703 (Pearce and Leng, 1996; Andersen, 1997; Goodenough *et al.*, 2002). So far, no evidence has been presented for an isotopically enriched mantle source in the Gardar Province as the existing ε_{Nd}(i) data of −0.5 to +5.2 show an isotopically depleted signature (Pearce and Leng, 1996; Andersen, 1997; Goodenough *et al.*, 2002, Upton *et al.*, 2003). Clinopyroxene from the EF samples of Paslick *et al.* (1993) yield ε_{Nd}(i) of +2.2. The Nd isotope data of this study are within the lower range of published values from the Gardar Province and extend the spread to more negative ε_{Nd}(i) values.

Several recent oxygen isotope studies have shown that mineral separates are less sensitive to low-*T* alteration and secondary water take-up than whole-rock samples (e.g. Vroon *et al.*, 2001). However, only few oxygen isotope data of mineral separates from continental volcanics are available (e.g. Dobosi *et al.*, 1998; Baker *et al.*, 2000). Extensive studies of mineral separates of ocean island basalts (Eiler *et al.*, 1997) and oceanic-arc lavas (Eiler *et al.*, 2000*a*) demon-

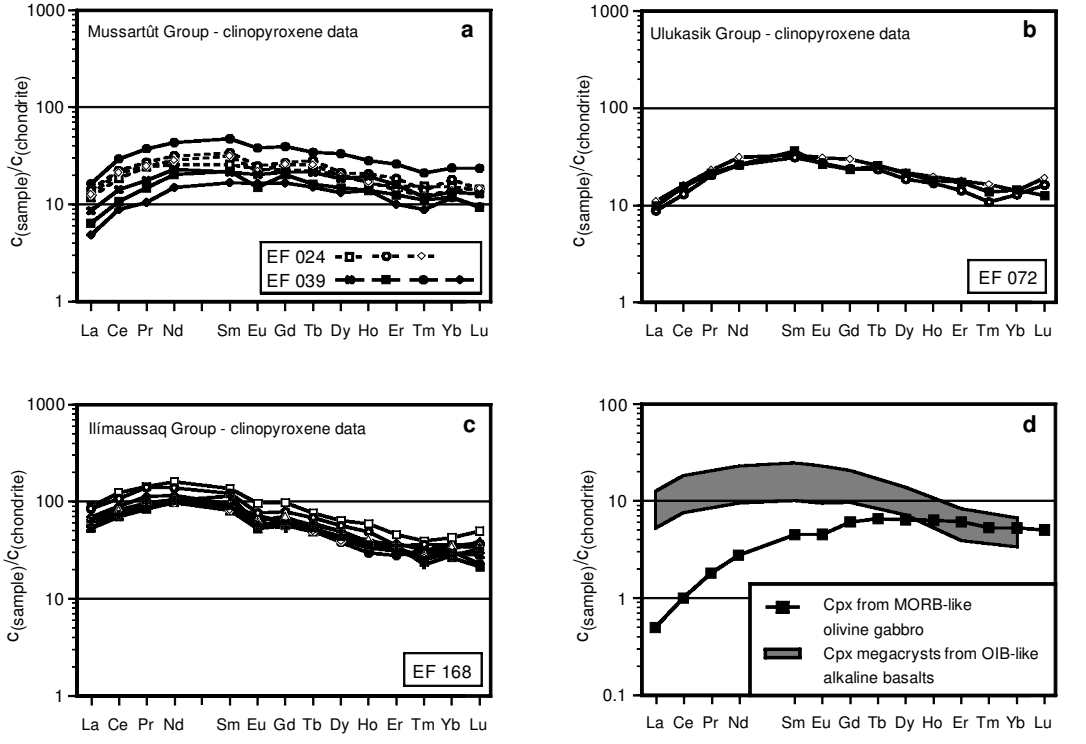

FIG. 6. *REE* patterns of clinopyroxenes (cpx) from Mussartût (*a*), Ulukasik (*b*) and Ilímaussaq (*c*) Group samples, normalized to chondritic values from Boynton (1984). (*d*) *REE* patterns of cpx from MORB-type olivine gabbro (Benoit *et al*., 1996) and OIB-type alkaline basalt (Nimis and Vannucci, 1995) for comparison (note the change of scale).

strated that analyses of mineral separates consistently span a narrower range than comparable whole-rock data. In our study, we used clinopyroxene because it is the only fresh mineral phase present in the samples. Oxygen isotope measurements of clinopyroxene separates from the EF basalts show a range in $\delta^{18}O_{cpx}$ from +5.2 to +6.0 ‰ with an average value of +5.66±0.23 (1σ) ‰. All samples overlap the range of $\delta^{18}O_{cpx}$ values from mantle peridotites (+5.25 to +5.90‰, Mattey *et al*., 1994), from continental flood basalts from Yemen (+5.5 to +6.9‰, Baker *et al*., 2000) and from alkaline basalts of Hungary (+5.07 to +5.34‰, Dobosi *et al*., 1998). There is a small difference between the averages of Mussartût Group ($\delta^{18}O_{cpx\text{-}avg}$ = +5.75±0.15 (1σ)‰) and Ulukasik Group ($\delta^{18}O_{cpx\text{-}avg}$ = +5.75±0.09 (1σ)‰) samples compared to Ilímaussaq Group ($\delta^{18}O_{cpx\text{-}avg}$ = +5.33±0.21 (1σ)‰) samples.

$\delta^{18}O$ values of melts coexisting with clinopyroxene were calculated assuming that oxygen in pyroxene and melt were in isotopic equilibrium and *T* was 1100ºC. $\Delta_{melt\text{-}cpx}$ can then be calculated using the following equation of Kalamarides (1986):

$$\Delta_{melt\text{-}cpx} = -0.0008T + 1.43 \ (T \text{ in Kelvin})$$

Although fractionation varies with magmatic temperatures, we consider the temperature of 1100ºC and the resulting $\Delta_{melt\text{-}cpx}$ of +0.3‰ as sufficiently representative considering the analytical errors involved. It is similar to $\Delta_{melt\text{-}cpx}$ values used in previous studies (+0.39‰: Vroon *et al*., 2001; +0.2‰: Dobosi *et al*., 1998). Resulting $\delta^{18}O_{melt}$ values of EF basalts range from +5.5 to +6.3‰. These values can be compared to whole-rock data from continental basalts given by Harmon and Hoefs (1995). Intraplate basalts from continental rift zones show a range from +4.6 to +8.3‰ with a mean of +6.1‰ and continental flood basalts, which are rather poorly represented in the database, have values between +4.3 and +6.5‰. Calculated EF

TABLE 4. Sr, Nd and O isotopic compositions of clinopyroxene separates from Eriksfjord Formation basalts. Whole-rock analyses from the Ketilidian basement and from sedimentary rocks of the Eriksfjord Formation are given for comparison.

Sample	Member	Sr (ppm)	Rb (ppm)	$^{87}Rb/^{86}Sr$	$^{87}Sr/^{86}Sr$	$^{87}Sr/^{86}Sr_{initial}$	Sm (ppm)	Nd (ppm)	$^{147}Sm/^{144}Nd$	$^{143}Nd/^{144}Nd$	$\varepsilon_{Nd}(i)$	$\delta^{18}O$
Basalts:												
EF 024	Mussartût	64.65	0.486	0.0218	0.704201±10	0.703826	7.38	22.80	0.1956	0.512467±10	− 3.2	5.67
EF 063	Mussartût											5.60±0.11
EF 061	Mussartût	89.95	0.999	0.0321	0.703818±10	0.703266	5.74	16.39	0.2115	0.512629±10	− 2.5	5.79±0.28
EF 039	Mussartût	73.74	0.583	0.0229	0.703492±10	0.703098	6.62	19.13	0.2092	0.512626±10	− 2.2	5.71±0.01
EF 059	Mussartût	54.47	0.137	0.0073	0.703375±12	0.703250	6.06	16.89	0.2171	0.512727±09	− 1.4	5.99±0.01
EF 108	Ulukasik	66.92	1.110	0.0480	0.703741±09	0.702916	10.99	36.82	0.1805	0.512617±10	+ 2.1	5.81
EF 072	Ulukasik	69.41	0.322	0.0134	0.703014±10	0.702784	8.18	25.19	0.1962	0.512574±10	− 1.2	5.68
EF 174	Ilímaussaq	125.4	2.324	0.0536	0.703935±10	0.703014	18.76	79.61	0.1424	0.512230±10	+ 0.4	5.47
EF 168	Ilímaussaq	86.67	1.422	0.0475	0.703799±07	0.702983	16.45	64.16	0.1550	0.512304±09	− 0.1	5.18
Basement and sedimentary rocks:												
JG 02	Julianehåb Granite	300.1	169.7	1.6375	0.744789±10	0.716647	10.53	62.28	0.1022	0.511470±09	−8.3	7.8
EF 021	Quartzite											11.5
EF 028	Arkosic arenite											6.8

Samples are listed in stratigraphic order from oldest to youngest. $^{87}Sr/^{86}Sr$ initial ratios and $\varepsilon_{Nd}(i)$ values were calculated for an age of 1.2 Ga. Standard deviations for $\delta^{18}O$ are given for samples that were analysed twice.

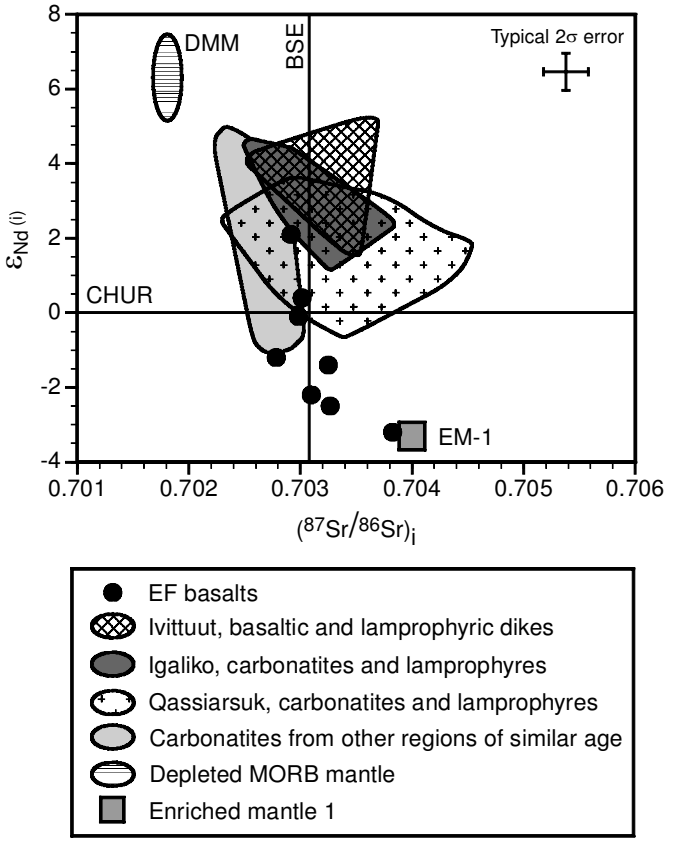

FIG. 7. $\varepsilon_{Nd}(i)$ *vs.* $(^{87}Sr/^{86}Sr)_i$ diagram, calculated for t = 1.2 Ga which is considered as the eruption age of the EF basalts (Paslick *et al.*, 1993). The reference line of Bulk Silicate Earth (BSE) for the Sr isotopic composition was calculated after DePaolo (1988) assuming present-day values of 0.0827 for $^{87}Rb/^{86}Sr$ and 0.7045 for $^{87}Sr/^{86}Sr$. Isotopic composition of the depleted MORB mantle (DMM) was calculated after DePaolo (1981), Goldstein *et al.* (1984) and Taylor and McLennan (1985). EM-1 was calculated after Schleicher *et al.* (1998) (see text for details). Data sources are: Goodenough *et al.* (2002), Ivittuut (n = 6); Pearce and Leng (1996), Igaliko (n = 5); Andersen (1997), Qassiarsuk (n = 25); Bell and Blenkinsop (1989), other carbonatites of similar age (Goudini, Schryburt Lake and Prairie Lake; n = 6).

model melt oxygen isotope data are within the ranges of both groups. Compared to Igaliko dyke rocks from further SE in the Gardar Province (Pearce and Leng, 1996), the EF basalts cover a much more restricted field, possibly because $\delta^{18}O$ whole-rock analyses are more prone to secondary alteration than analyses of mineral separates (Fig. 8). Whole-rock $\delta^{18}O$ measurements of the underlying Julianehåb Granite and of the sedimentary sandstone members of the Eriksfjord Formation yield values of 7.8‰ and 6.8–11.5‰, respectively (Table 4), and are shown for comparison.

Discussion

Mantle source regions of the EF basalts

To reconstruct the mantle sources involved in the formation of the EF basalts, we use Sr-Nd-O isotope and incompatible trace element data. On a Sr-Nd isotope diagram, the isotopic composition of DMM was modelled for an age of 1.2 Ga (DePaolo 1981; Goldstein *et al.*, 1984; Taylor and McLennan, 1985). The fairly constant $^{87}Sr/^{86}Sr$ initial isotope ratios of the EF basalts are ~0.703 which falls within the range typical for mantle-derived rocks, but slightly above calculated values for DMM (Fig. 7). $\varepsilon_{Nd}(i)$ values are more

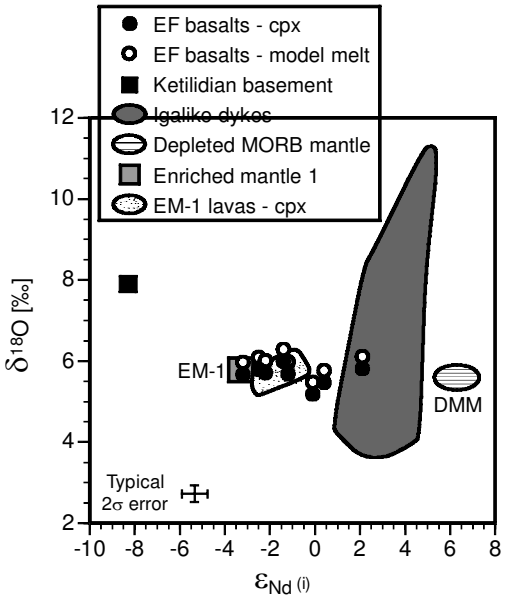

FIG. 8. Oxygen isotopic compositions ($\delta^{18}O$‰ V-SMOW) of clinopyroxene from EF basalts, calculated melt (see text for details) and whole-rock Ketilidian basement *vs*. $\varepsilon_{Nd}(i)$. Whole-rock data for Igaliko dyke rocks (n = 7) are from Pearce and Leng (1996), DMM data derived from fresh MORB glasses are from Eiler *et al.* (2000*b*). The field of EM-1 lavas is taken from clinopyroxene data of Gough and Tristan da Cunha Island lavas (Harris *et al*., 2000) and the EM-1 end-member composition is based on the calculations after Schleicher *et al.* (1998) for $\varepsilon_{Nd}(i)$ and an average value of 5.78‰ (n = 18) from the EM-1 lavas for $\delta^{18}O$.

scattered and indicate that the rocks contain a mixture of isotopic components from both mantle and crustal reservoirs or a heterogeneous mantle source. Only one sample (EF 108) has an $\varepsilon_{Nd}(i)$ value significantly above 0. This sample exhibits the largest spread of clinopyroxene compositions, which may reflect strong alteration. Goodenough *et al.* (2002) also note that the highest ε_{Nd} occurs in the most altered sample of their sample set. However, Paslick *et al.* (1993) report clinopyroxene data from two Ulukasik Group samples with $\varepsilon_{Nd}(i) > +2$, and those samples were apparently not disturbed with regard to their Sm-Nd age information. On the other hand, Piper *et al.* (1999) suggest that the Sm-Nd systematics of those samples may be erroneous due to later disturbance by fluids derived from the Ilímaussaq intrusion. Therefore, although we are presently not able to decide whether positive $\varepsilon_{Nd}(i)$ values for the EF basalts are real, it is clear that none of those values is close to values of a 1.2 Ga old DMM source (i.e. ε_{Nd} = +5 to +7).

The Sr-Nd isotopic composition for OIB-type sources in the Proterozoic is not as well constrained as DMM. Today, OIB-type mantle sources have a wide range of isotopic compositions that partly overlap with DMM, but ε_{Nd} values are generally lower (Hart *et al*., 1992; Hofmann, 1997). The EM-1 mantle component is characterized by extremely low $^{143}Nd/^{144}Nd$ ratios and ε_{Nd} values of between 0 and −5 (Hofmann, 1997). A possible 1.2 Ga position for EM-1 is plotted in Fig. 7, calculated according to Schleicher *et al.* (1998) with $^{147}Sm/^{144}Nd = 0.18$ and $^{87}Rb/^{86}Sr = 0.10$. The present-day values used in the calculation are $^{143}Nd/^{144}Nd = 0.51234$ and $^{87}Sr/^{86}Sr = 0.7057$, taken from ocean island basalts closest to an EM-1 end-member (Hofmann, 1997). Other Sr-Nd isotope data from the Gardar Province are plotted to put further constraints on the mantle sources of the EF basalts (Fig. 7). We also added comparative data from African and Canadian carbonatites of similar age because there is a well known similarity between Sr-Nd isotopic data of OIBs and carbonatites (Bell and Blenkinsop, 1989). The linear array of the carbonatite data is considered to be the result of mixing between the two mantle components HIMU and EM-1 (Bell and Blenkinsop, 1989; Bell and Tilton, 2001). The carbonatites from the Gardar Province have similar Nd but slightly more radiogenic Sr isotopic compositions than the reference carbonatite data (Fig. 7). The least contaminated samples overlap with the linear array and the more radiogenic Sr isotopic composition can be explained by crustal contamination (Andersen, 1997). We therefore consider it possible that the Gardar carbonatites also represent mixing of hypothetical HIMU and EM-1 components of an OIB-like source. Since the isotopically most primitive EF basalt samples overlap with the Qassiarsuk carbonatites, it could be possible that the basalts also contain such mantle components, although Pb isotope data for the EF basalts that could clarify the importance of a HIMU source are lacking. Based on the Sr-Nd isotope data, the EF basalts appear to be derived from a heterogeneous OIB-like mantle source that comprises isotopically depleted and enriched components. OIB-like and carbonatitic magmatism are often attributed to mantle plume activity (Bell and Simonetti, 1996; Hofmann, 1997;

Simonetti *et al.*, 1998). A plume input to the formation of the EF basalts is supported by the relatively large volume of magmas and the short duration (<5 Ma) of magmatism (Piper *et al.*, 1999). It is also compatible with the geological setting of a continental breakup. Additionally, a plume component appears to be necessary to explain the thermal input, as it is difficult to melt a cold lithosphere section (Arndt and Christensen, 1992).

Oxygen isotope data of the EF basalts are generally consistent with a mantle derivation, including an OIB-like mantle source. On the $\delta^{18}O$ *vs.* $\varepsilon_{Nd}(i)$ diagram (Fig. 8), the overlap between the EF data, clinopyroxene data from EM-1-like oceanic basalts and the hypothetical EM-1 end-member suggests an involvement of an EM-1-type mantle source. Olivines from HIMU-like sources are known to be slightly lower in $\delta^{18}O$ than typical upper mantle values from MORBs (Eiler *et al.*, 1997), but the EF data are not sufficient to assess if the slightly lower $\delta^{18}O$ values in the Ilímaussaq Group basalts are caused by a relatively higher input from a HIMU source.

The contribution of the various mantle sources to the EF basalts can also be evaluated on the primitive mantle-normalized multi-element diagram (Fig. 4) and on the *REE* plots (Figs 5 and 6). Both the whole-rock *REE* and the clinopyroxene *REE* patterns of the EF basalts are unlike those representative of N-MORB sources. We conclude again that DMM did not play a major role in the petrogenesis of the EF basalts. On the other hand, similarities with OIB-like mantle sources are more prominent. The shape of the clinopyroxene *REE* pattern closely resembles those from clinopyroxene of OIB-like alkaline basalts, despite differences in absolute concentrations. The whole-rock *REE* patterns of the EF basalts lie between E-MORB and average OIB patterns, as do the multi-element patterns. On the latter, the EF basalts have marked positive Ba and P peaks that are not present in typical OIBs. However, Ba contents should be interpreted with caution since highly variable Zr/Ba ratios from 0.14 to 0.70 are an indication that Ba was re-mobilized after emplacement of the basalts (e.g. Price *et al.*, 1991; Oliveira and Tarney, 1995). Likewise, P mobility was demonstrated in altered basaltic rocks (Winchester and Floyd, 1976). In summary, the *REE* and trace element data are evidence that the mantle source(s) of the EF basalts were enriched in incompatible trace elements relative to primitive mantle.

For relatively primitive *hy*-normative basaltic rocks of the Ivittuut area further north in the Gardar Province, it has been argued that some of them were derived from a lithospheric mantle source previously enriched by subduction-related processes. This interpretation is based on certain geochemical characteristics such as high La/Nb ratios and negative Nb anomalies (Goodenough *et al.*, 2002). For the EF basalts, negative Nb anomalies are not clearly discernible, but La/Nb ratios are >1 which seems to be a characteristic feature of a lithospheric mantle source (Fitton, 1995). La/Ba, La/Rb and La/K ratios were also used to argue for a lithospheric origin of the Gardar basic magmas, although a mantle plume involvement was assumed to provide the required energy (Upton and Emeleus, 1987; Upton *et al.*, 2003). Since feldspar is the only primary magmatic mineral in the EF basalts in which Ba, Rb and K are incorporated in significant amounts and the feldspars are generally altered, these elements might have been easily mobilized and we therefore do not dare to base the interpretation of the EF basalts sources on these data. In addition, the lack of precise geochemical data on the composition of the lithosphere below the Gardar Province complicates an evaluation of the lithospheric contribution to the EF basaltic magmatism.

Certain ratios of incompatible trace elements of the EF basalts are compared to several occurrences of ocean island basalts representative of EM-1 and HIMU sources in Table 5. Ratios between highly incompatible trace elements do not change significantly during partial melting or fractional crystallization in basaltic systems and may therefore constrain the ratios in their sources (Weaver *et al.*, 1987). The EF basalts are subdivided into the more alkaline, isotopically primitive Ilímaussaq Group samples and those samples with $\varepsilon_{Nd}(i) < -1$. The Ilímaussaq Group samples have higher Sr/Nd, La/Nb and Zr/Nb ratios than HIMU and overlap with the upper range of EM-1 ratios. The EF basalts with $\varepsilon_{Nd}(i) < -1$ have generally higher ratios than the oceanic island basalts and partly overlap with typical values of the lower crust. It therefore seems likely that assimilation of lower crustal material may have changed the primary trace element ratios in the basalts. Therefore, we will evaluate the possible influence of assimilation of crustal material on the geochemistry of the EF basalts in the following section.

TABLE 5. Trace element ratios of EF basalts compared to ocean island basalts (OIBs) representing EM-1 and HIMU mantle components, and the lower crust.

	Sr/Nd	La/Nb	Zr/Nb
EF basalts with $\varepsilon_{Nd} < -1$	24.9 – 39.6	1.20 – 1.50	12.1 – 15.7
Ilímaussaq Group EF basalts	19.8 – 29.2	1.04 – 1.19	5.1 – 5.3
EM-1	9.0 – 20.7	0.67 – 1.11	3.9 – 10.9
HIMU	4.5 -16.3	0.63 – 0.80	2.7 – 3.6
Lower continental crust	30	1.6	13.6

Data sources: EM-1: Humphris and Thompson (1983, Walvis Ridge) and Cliff *et al.* (1991, Inaccessible Islands); HIMU: Chauvel *et al.* (1992, Tubuai Island); Lower continental crust: Rudnick and Fountain (1995).

The role of crustal contamination

Large amounts of bulk assimilation of crustal material, which is relatively SiO_2-rich compared to a basaltic melt, would drive the compositions to higher SiO_2 contents and quartz-normative compositions. Partial melts derived from crustal rocks would also be relatively SiO_2-rich (Beard *et al.*, 1993; Carroll and Wyllie, 1990) and would have the same effect. The *ne*-normative character of the EF basalts (Table 1) suggests that assimilation of crustal material, especially of silica-rich upper crustal rocks, was not significant with the possible exception of sample EF 059.

On the primitive mantle-normalized multi-element diagrams (Fig. 4), Ti troughs are typical for crustal rocks, especially for the Upper Crust (Rudnick and Fountain, 1995) and they may therefore be present in rocks extensively contaminated by continental crust. Ti troughs are generally lacking in the patterns of the EF basalts and a major upper crustal contribution to the magmas can therefore be excluded. However, small amounts of assimilation of lower crustal material cannot be ruled out because the average lower crust has higher Ti contents.

Steep trends on Sr-Nd isotope plots have been attributed to assimilation of granulite-facies gneisses (e.g. Bernstein *et al.*, 1998). AFC modelling based on an equation developed by DePaolo (1981) was performed to test the hypothesis of small amounts of contamination with lower crustal material (Fig. 9). The basaltic magma which represents one end-member for the calculations has the isotopic signature of the isotopically most primitive samples from the present data set and from the literature (Table 6). Two possible contaminants representing upper and lower crustal compositions were selected for modelling (Table 6). The representative samples are a granite from the Julianehåb batholith for the upper crust (sample JG 02) and an average of five granulite-facies gneisses with low Rb/Sr ratios from the Archaean craton of West Greenland (Taylor *et al.*, 1984) for

TABLE 6. End-member compositions used for AFC modelling.

End-member	Sr (ppm)	$(^{87}Sr/^{86}Sr)_i$ (T = 1.2 Ga)	Nd (ppm)	$\varepsilon_{Nd}(i)$ (T = 1.2 Ga)	Data source
Primitive EF basaltic magma	507	0.70278	18	+ 2.2	Sample EF 072, Paslick *et al.* (1993)
Upper crust (Julianehåb Granite)	300	0.71665	62	–8.3	Sample JG 02
Lower crust* (Granulite facies gneiss)	747	0.70668	63	–23.4	Taylor *et al.* (1984)

* The composition of the granulite-facies gneiss is an average of 5 samples with low Rb/Sr ratios <0.2.

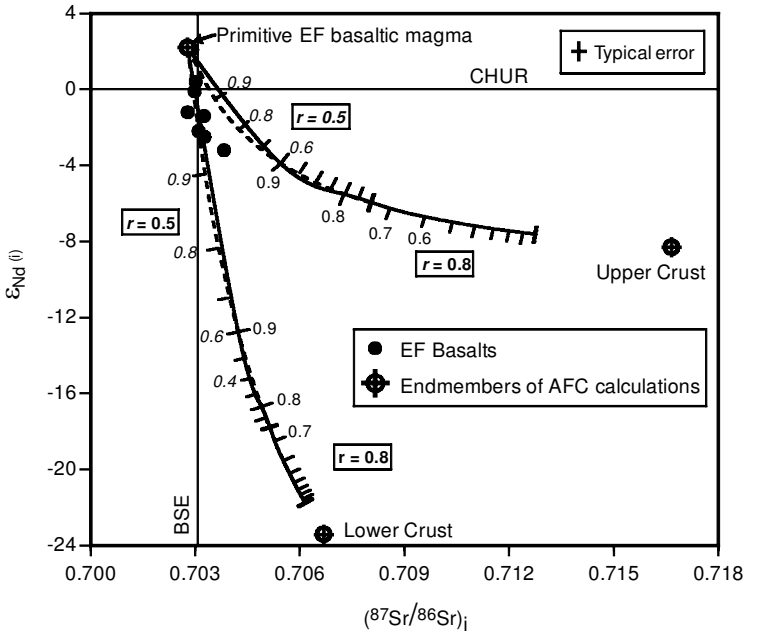

FIG. 9. $\varepsilon_{Nd}(i)$ *vs.* $(^{87}Sr/^{86}Sr)_i$ diagram showing the results of AFC modelling. End-member compositions are listed in Table 6. Olivine is the only fractionating mineral. Partition coefficients for olivine/melt are from the compilation of Rollinson (1993). Curves were calculated for two values of r (r = rate of assimilation/rate of fractional crystallization). Dashed lines and numbers in italics are for r = 0.5, solid lines and regular numbers are for r = 0.8. Values at the curves are for F values (fraction of melt remaining) with 10% tick marks.

the lower crust. An influence of Archaean rocks on Gardar magmas has been demonstrated by Pb isotope studies (Taylor and Upton, 1993) and seismic data were also interpreted to reflect the existence of a wedge of Archaean crust that extends southwards to Lindenow Fjord (Dahl-Jensen *et al.*, 1998). We have shown in the previous sections, on the basis of Ni trends, that fractionation of olivine was most relevant to the major element evolution of the lavas, whereas fractionation of other phases was apparently of minor importance. We therefore modelled the AFC processes with olivine fractionation using mineral-melt partition coefficients of 0.014 for Sr and 0.0066 for Nd (Rollinson, 1993).

The modelling of AFC processes is strongly dependent on the parameter r, defined as the ratio of mass assimilation rate and fractional crystallization rate (DePaolo, 1981). The change in isotopic signature becomes enhanced for higher values of r. Reiners *et al.* (1995) have shown that r values might be very high and even >1 in the early stages of magmatic evolution at high temperatures since crystallization can be suppressed by assimilation. Therefore, we calculated AFC processes with two r values of 0.5 and 0.8 that represent a relatively high and a middle to low assimilation rate to demonstrate the effects of variable r (Fig. 9). The results indicate that AFC processes involving upper crust similar to the Julianehåb Granite cannot explain the trend of the EF basalts because Sr isotopic compositions would shift to considerably more radiogenic values. This result is consistent with the conclusions derived from trace element data. The AFC curves for assimilation of lower crust, however, agree well with the bulk of the data. The most negative ε_{Nd} values can be explained by AFC processes with intermediate assimilation rates (r = 0.5) involving assimilation of <5% lower crustal material. With a greater degree of assimilation and an r value of 0.8, <4% assimilation is indicated.

Lower crustal rocks of igneous origin have an average $\delta^{18}O$ value of +7.5±1.4‰ with an overall range from +5.4 to +12.5‰ (Fowler and Harmon, 1990). 5 to 10% bulk assimilation of lower crustal material with $\delta^{18}O$ = +7.5‰ into a typical mantle-derived magma with $\delta^{18}O$ = +5.7‰ results in $\delta^{18}O$ values of the contaminated magma from

+5.79 to +5.88‰. Therefore, the $\delta^{18}O$ data cannot be used to rule out small amounts of assimilation of lower crust. To evaluate how much contamination would be permissible from the present oxygen isotope data, we calculated how much contamination of a mantle-derived magma with ^{18}O = +5.7‰ with a contaminant within the lower range of lower crustal xenoliths ($\delta^{18}O$ = +6.7‰) would drive the oxygen isotopic composition to the highest value of the EF basalts ($\delta^{18}O$ ~+6.3‰). Although simple mixing shows that 60% assimilation is permissible, this amount would drive the whole-rock geochemistry to more silicic compositions than is observed in the EF basalts. In Fig. 8, there is no obvious trend from the basalts towards the Ketilidian basement, suggesting again that upper crust was not assimilated in significant amounts.

Ratios of trace elements incompatible in basaltic systems can be used to distinguish between crust and mantle reservoirs (e.g. Weaver, 1991). Based on the AFC modelling, EF basalts with $\varepsilon_{Nd}(i) < -1$ are those which are most likely influenced by crustal contamination. The relatively high La/Nb and Zr/Nb ratios of these samples are consistent with assimilation of lower crustal material. Sr/Nd ratios are even higher than the average lower crustal composition, but Sr/Nd ratios in those samples which were taken as representative for the lower crust in the AFC modelling can reach values of 80, i.e. well above the highest EF basalt ratios. Again, the Sr/Nd ratios support the hypothesis of some lower crustal contamination.

The absence of more primitive basaltic rocks with MgO >8 wt.% might also indicate lower crustal assimilation. It suggests that magmas may have been retained at depth where they acquired more evolved compositions by fractional crystallization and had the opportunity to assimilate lower crustal material during crustal underplating (Upton *et al.*, 2003).

Summary and conclusions

The new geochemical data of the Eriksfjord Formation basalts in the Gardar Province provided in this study are used to place petrogenetic constraints on the sources of their parental magmas. Based on trace-element patterns and Sr-Nd isotopic constraints, there seems to be no indication that a DMM-like source played an important role in magma genesis of the EF basalts. Clinopyroxene and whole-rock *REE* patterns are more compatible with an OIB-like source, but we are not able to conclude whether the observed enrichment in *REE* reflects the source's signature or magmatic processes. The isotopically most primitive EF basalts have Sr-Nd isotopic compositions that are similar to Gardar carbonatites. Due to the isotopic similarity between carbonatites and OIBs, many are thought to be related to mantle plumes (Bell, 2001). We therefore speculate that OIB-like mantle components from a plume source were also involved in the parental EF magmas, but we cannot exclude interaction with the SCLM. Two distinct mantle components, one isotopically depleted and another one enriched, could have contributed to the EF magmas. AFC modelling of Sr-Nd isotope data indicates that assimilation of <5% lower crust could explain the steep vector on the Sr-Nd isotope plot, but assimilation of upper crustal material is unlikely. Oxygen isotope data of clinopyroxene separates are consistent with a mantle origin but permit some assimilation of lower crustal rocks. In summary, the data are consistent with the hypothesis that the EF magmas could have originated from a mantle plume source, which is supported by geological arguments, and that they underwent some assimilation of lower crustal material.

Acknowledgements

We would like to thank Bruce Paterson who provided invaluable help during Laser ICP-MS measurements at the Large-Scale Geochemical Facility supported by the European Community-Access to Research Infrastructure action of the Improving Human Potential Programme, contract number HPRI-CT-1999-00008 awarded to Prof. B.J. Wood (University of Bristol). Gabi Stoschek and Torsten Vennemann are thanked for their help with oxygen isotope measurements. Elmar Reitter expertly assisted with preparation and measurements of radiogenic isotopes and Mathias Westphal helped with microprobe measurements. *REE* whole-rock analyses were kindly provided by the NERC facility at Royal Holloway, University of London. Michael Marks is thanked for his pleasant company during fieldwork. Very constructive reviews by Tom Andersen and Alexei S. Rukhlov greatly helped to improve the manuscript. We also thank Ian Coulson for final editing. Funding of this work by the Deutsche Forschungsgemeinschaft (grant Ma-2135/1-2) is gratefully acknowledged.

References

Andersen, T. (1997) Age and petrogenesis of the Qassiarsuk carbonatite-alkaline silicate volcanic complex in the Gardar rift, South Greenland. *Mineralogical Magazine*, **61**, 499–513.

Armstrong, J.T. (1991) Quantitative elemental analysis of individual microparticles with electron beam instruments. Pp. 261–315 in: *Electron Probe Quantitation* (K.F.J. Heinrich and D.E. Newbury, editors). Plenum Press, New York and London.

Arndt, N.T. and Christensen, U. (1992) The role of lithospheric mantle in continental flood volcanism: Thermal and geochemical constraints. *Journal of Geophysical Research*, **97**, 10967–10981.

Baker, J.A., Menzies, M.A., Thirlwall, M.F. and Macpherson, C.G. (1997) Petrogenesis of Quaternary Intraplate Vocanism, Sana'a, Yemen: Implications for Plume-Lithosphere Interaction and Polybaric Melt Hybridization. *Journal of Petrology*, **38**, 1359–1390.

Baker, J.A., MacPherson, C.G., Menzies, M.A., Thirlwall, M.F., Al-Kadasi, M. and Mattey, D.P. (2000) Resolving crustal and mantle contributions to continental flood volcanism, Yemen; constraints from mineral oxygen isotope data. *Journal of Petrology*, **41**, 1805–1820.

Beard, J.S., Abitz, R.J. and Lofgren, G.E. (1993) Experimental melting of crustal xenoliths from Kilbourne Hole, New Mexico and implications for the contamination and genesis of magmas. *Contributions to Mineralogy and Petrology*, **115**, 88–102.

Bell, K. (2001) Carbonatites; relationships to mantle-plume activity. *Geological Society of America Special Paper,* **352**, 267–290.

Bell, K. and Blenkinsop, J. (1989) Neodymium and Strontium Isotope Geochemistry of Carbonatites. Pp. 278–300 in: *Carbonatites – Genesis and Evolution* (K. Bell, editor). Unwin Hyman, London.

Bell, K. and Simonetti, A. (1996) Carbonatite Magmatism and Plume Activity: Implications from the Nd, Pb and Sr Isotope Systematics of Oldoinyo Lengai. *Journal of Petrology*, **37**, 1321–1339.

Bell, K. and Tilton, G.R. (2001) Nd, Pb and Sr Isotopic Compositions of East African Carbonatites: Evidence for Mantle Mixing and Plume Inhomogeneity. *Journal of Petrology*, **42**, 1927–1945.

Benoit, M., Polvé, M. and Ceuleneer, G. (1996) Trace element and isotopic characterization of mafic cumulates in a fossil mantle diapir (Oman ophiolite) *Chemical Geology*, **134**, 199–214.

Bernstein, S., Kelemen, P.B., Tegner, C., Kurz, M.D., Blusztajn, J. and Kent Brooks, C. (1998) Post-breakup basaltic magmatism along the East Greenland Tertiary rifted margin. *Earth and Planetary Science Letters*, **160**, 845–862.

Boynton, W.V. (1984) Geochemistry of the rare earth elements: meteorite studies. Pp. 63–114 in: *Rare Earth Element Geochemistry* (P. Henderson, editor). Elsevier, Amsterdam.

Carroll, M.R. and Wyllie, P.J. (1990) The system tonalite-H_2O at 15 kbar and the genesis of calc-alkaline magmas. *American Mineralogist*, **75**, 345–357.

Chauvel, C., Hofmann, A.W. and Vidal, P. (1992) HIMU-EM: The French Polynesian connection. *Earth and Planetary Science Letters*, **110**, 99–119.

Clayton, R.N. and Mayeda, T.K. (1963) The use of bromine pentafluoride in the extraction of oxygen from oxides and silicates for isotope analysis. *Geochimica et Cosmochimica Acta*, **27**, 43–52.

Coulson, I.M. and Chambers, A.D. (1996) Patterns of zonation in rare-earth-bearing minerals in nepheline syenites of the North Qôroq center, South Greenland. *The Canadian Mineralogist*, **34**, 1163–1178.

Cox, K.G., Bell, J.D. and Pankhurst, R.J. (1979) *The Interpretation of Igneous Rocks*. George, Allen and Unwin, London.

Cross, W., Iddings, J.P., Pirsson, L.V. and Washington, H.S. (1903) *Quantitative Classification of Igneous Rocks.* University of Chicago Press.

Dahl-Jensen, T., Thybo, T., Hopper, H. and Rosing, M. (1998) Crustal structure at the SE Greenland margin from wide-angle and normal incidence seismic data. *Tectonophysics*, **288**, 191–198.

DePaolo, D.J. (1981) Trace element and isotopic effects of combined wallrock assimilation and fractional crystallisation. *Earth and Planetary Science Letters*, **53**, 189–202.

DePaolo, D.J. (1988) *Neodymium Isotope Geochemistry: An Introduction.* Springer-Verlag, New York.

Dobosi, G., Downes, H., Mattey, D. and Embey-Isztin, A. (1998) Oxygen isotope ratios of phenocrysts from alkali basalts of the Pannonian basin: Evidence for an O-isotopically homogeneous upper mantle beneath a subduction-influenced area. *Lithos*, **42**, 213–223.

Eiler, J.M. (2001) Oxygen isotope variations of basaltic lavas and upper mantle rocks. Pp. 319–364 in: *Stable Isotope Geochemistry* (J.W. Valley and D.R. Cole, editors). Reviews in Mineralogy and Geochemistry, **43**. The Mineralogical Society of America, Washington D.C.

Eiler, J.M., Farley, K.A., Valley, J.W., Hauri, E., Craig, H., Hart, S.R. and Stolper, E.M. (1997) Oxygen isotope variations in ocean island basalt phenocrysts. *Geochimica et Cosmochimica Acta*, **61**, 2281–2293.

Eiler, J.M., Crawford, A., Elliot, T., Farley, K.A., Valley, J.W. and Stolper, E.M. (2000*a*) Oxygen isotope geochemistry of oceanic-arc lavas. *Journal*

of Petrology, **41**, 229–256.

Eiler, J.M., Schiano, P., Kitchen, N. and Stolper, E.M. (2000*b*) Oxygen-isotope evidence for recycled crust in the sources of mid-ocean-ridge basalts. *Nature*, **403**, 530–534.

Emeleus, C.H. and Upton, B.G.J. (1976) The Gardar period in southern Greenland. Pp. 152–181 in: *Geology of Greenland* (A. Escher and W.S. Watt, editors). Geological Survey of Greenland, Copenhagen.

Fitton, J.G. (1995) Coupled molybdenum and niobium depletion in continental basalts. *Earth and Planetary Science Letters*, **136**, 715–721.

Fitton, J.G., Saunders, A.D., Norry, M.J., Hardarson, B.S. and Taylor, R.N. (1997) Thermal and chemical structure of the Iceland plume. *Earth and Planetary Science Letters*, **153**, 197–208.

Floyd, P.A. and Winchester, J.A. (1975) Magma-type and tectonic setting discrimination using immobile elements. *Earth and Planetary Science Letters*, **27**, 211–218.

Fowler, M.B. and Harmon, R.S. (1990) The oxygen isotope composition of lower crustal granulite xenoliths. Pp. 493–506 in: *Granulites and Crustal Evolution* (D.Vielzeuf and P. Vidal, editors). Kluwer Academic Publishers, Dordrecht, The Netherlands.

Garde, A.A., Hamilton, M.A., Chadwick, B., Grocott, J. and McCaffrey, K.J.W. (2002) The Ketilidian orogen of South Greenland: geochronology, tectonics, magmatism, and fore-arc accretion during Palaeoproterozoic oblique convergence. *Canadian Journal of Earth Sciences*, **39**, 765–793.

Gibson, S.A., Thompson, R.N., Dickin, A.P. and Leonardos, O.H. (1995) High-Ti and Low-Ti mafic potassic magmas: key to plume-lithosphere interactions and continental flood-basalt genesis. *Earth and Planetary Science Letters*, **136**, 149–165.

Gibson, S.A., Thompson, R.N., Weska, R.K. and Dickin, A.P. (1997) Late-Cretaceous rift-related upwelling and melting of the Trinidade starting mantle-plume head beneath western Brazil. *Contributions to Mineralogy and Petrology*, **126**, 303–314.

Gibson, S.A., Thompson, R.N., Leonardos, O.H., Dickin, A.P. and Mitchell, J.G. (1999) The limited extent of plume-lithosphere interactions during continental flood-basalt genesis: geochemical evidence from Cretaceous magmatism in southern Brazil. *Contributions to Mineralogy and Petrology*, **137**, 147–169.

Goldstein, S.L., O'Nions, R.K. and Hamilton, P.J. (1984) A Sm-Nd isotopic study of the atmospheric dust and particulates from major river systems. *Earth and Planetary Science Letters*, **70**, 221–236.

Goodenough, K.M., Upton, B.G.J. and Ellam, R.M. (2002) Long-term memory of subduction processes in the lithospheric mantle: evidence from the geochemistry of basic dykes in the Gardar Province of south Greenland. *Journal of the Geological Society of London*, **159**, 705–714.

Harmon, R.S. and Hoefs, J. (1995) Oxygen isotope heterogeneity of the mantle deduced from global ^{18}O systematics of basalts from different geotectonic settings. *Contributions to Mineralogy and Petrology*, **120**, 95–114.

Harris, C., Smith, H.S. and le Roex, A.P. (2000) Oxygen isotope composition of phenocrysts from Tristan da Cunha and Gough Island lavas: variation with fractional crystallization and evidence for assimilation. *Contributions to Mineralogy and Petrology*, **138**, 164–175.

Hart, S.R., Hauri, E.H., Oschmann, L.A. and Whitehead, J.A. (1992) Mantle plumes and entrainment: Isotopic evidence. *Science*, **256**, 517–520.

Hawkesworth, C.J., Kempton, P.D., Rogers, N.W., Ellam, R.M. and van Calsteren, P.W. (1990) Continental mantle lithosphere and shallow level enrichment processes in the Earth's mantle. *Earth and Planetary Science Letters*, **96**, 256–268.

Heaman, L.M. and Machado, N. (1992) Timing and origin of midcontinent rift alkaline magmatism, North America: evidence from the Coldwell Complex. *Contributions to Mineralogy and Petrology*, **110**, 289–303.

Hofmann, A. (1997) Mantle geochemistry: the message from oceanic volcanism. *Nature*, **385**, 219–229.

Humphris, S.E. and Thompson, G. (1983) Geochemistry of rare earth elements in basalts from the Walvis Ridge: implications for its origin and evolution. *Earth and Planetary Science Letters*, **66**, 223–242.

Jacobsen, S.B. and Wasserburg, G.J. (1980) Sm-Nd isotopic evolution of chondrites. *Earth and Planetary Science Letters*, **50**, 139–155.

Kalamarides, R.I. (1986) High-temperature oxygen isotope fractionation among the phases of Kiglapait intrusion, Labrador, Canada. *Chemical Geology*, **58**, 303–310.

Larsen, J.G. (1977) Petrology of the late lavas of the Eriksfjord Formation, Gardar province, South Greenland. *Bulletin Grønlands Geologiske Undersøgelse*, **125**, 31 pp.

Le Maitre, R.W., Bateman, P., Dudek, A., Keller, J., Le Bas, M.J., Sabine, P.A., Schmid, R., Sørensen, H., Streckeisen, A., Woolley, A.R. and Zanettin, B. (1989) *A Classification of Igneous Rocks and Glossary of Terms*. Blackwell, Oxford, UK.

Lightfoot, P.C., Sutcliffe, R.H. and Doherty, W. (1991) Crustal contamination identified in Keweenawan Osler Group Tholeiites, Ontario: A trace element perspective. *Journal of Geology*, **99**, 739–760.

Lindsley, D.H. (1983) Pyroxene thermometry. *American Mineralogist*, **68**, 477–493.

Lugmair, G.W. and Marti, K. (1978) Lunar initial

$^{143}Nd/^{144}Nd$: differential evolution of the lunar crust and mantle. *Earth and Planetary Science Letters*, **39**, 349–357.

Mahoney, J.J. (1988) Deccan traps. Pp. 151–194 in: *Continental Flood Basalts* (J.D. MacDougall, editor). Kluwer Academic Publishers, Dordrecht, The Netherlands.

Mattey, D., Lowry, D. and Macpherson, C. (1994) Oxygen isotope composition of mantle peridotite. *Earth and Planetary Science Letters*, **128**, 231–241.

McDonough, W.F. and Sun, S.S. (1995) The composition of the Earth. *Chemical Geology*, **120**, 223–253.

Middlemost, E.A.K. (1989) Iron oxidation ratios, norms and the classification of volcanic rocks. *Chemical Geology*, **77**, 19–26.

Molzahn, M., Reisberg, L. and Wörner, G. (1996) Os, Sr, Nd, Pb, O isotope and trace element data from the Ferrar flood basalts, Antarctica: evidence for an enriched subcontinental lithospheric source. *Earth and Planetary Science Letters*, **144**, 529–546.

Morimoto, N., Fabrie, J., Ferguson, A.K., Ginzburg, I.V., Ross, M., Seifert, F.A., Zussman, J., Aoki, K. and Gottardi, G. (1988) Nomenclature of pyroxenes. *Mineralogical Magazine*, **52**, 535–550.

Nicholson, S.W., Shirey, S.B., Schulz, K.J. and Green, J.C. (1997) Rift-wide correlation of 1.1 Ga Midcontinent rift system basalts: implications for multiple mantle sources during rift development. *Canadian Journal of Earth Sciences*, **34**, 504–520.

Nimis, P. and Vannucci, R. (1995) An ion microprobe study of clinopyroxenes in websteritic and megacrystic xenoliths from Hyblean Plateau (SE Sicily, Italy): constraints on HFSE/REE/Sr fractionation at mantle depth. *Chemical Geology*, **124**, 185–197.

Oliveira, E.P. and Tarney, J. (1995) Petrogenesis of the Late Proterozoic Curaçá mafic dyke swarm, Brazil: asthenospheric magmatism associated with continental collision. *Mineralogy and Petrology*, **53**, 27–48.

Ormerod, D.S., Hawkesworth, C.J., Rogers, N.W., Leeman, W.P. and Menzies, M.A. (1988) Tectonic and magmatic transitions in the Western Great Basin, USA. *Nature*, **333**, 349–353.

Paces, J.B. and Bell, K. (1989) Non-depleted subcontinental mantle beneath the Superior Province of the Canadian Shield: Nd-Sr isotopic and trace element evidence from Midcontinent Rift basalts. *Geochimica et Cosmochimica Acta*, **53**, 2023–2035.

Paslick, C.R., Halliday, A.N., Davies, G.R., Mezger, K. and Upton, B.G.J. (1993) Timing of proterozoic magmatism in the Gardar Province, southern Greenland. *Bulletin of the Geological Society of America*, **105**, 272–278.

Paslick, C.R., Halliday, A.N., James, D. and Dawson, J.B. (1995) Enrichment of the continental lithosphere by OIB melts: Isotopic evidence from the volcanic province of northern Tanzania. *Earth and Planetary Science Letters*, **130**, 109–126.

Pearce, N.J.G. and Leng, M.J. (1996) The origin of carbonatites and related rocks from the Igaliko Dyke Swarm, Gardar Province, South Greenland: field, geochemical and C-O-Sr-Nd isotope evidence. *Lithos*, **39**, 21–40.

Perry, F.V., Baldridge, W.S. and DePaolo, D.J. (1987) Role of asthenosphere and lithosphere in the genesis of late cenozoic basaltic rocks from the Rio Grande rift and adjacent regions of the Southwestern United States. *Journal of Geophysical Research*, **92**, 9193–9213.

Philpotts, A.R. (1990) *Principles of Igneous and Metamorphic Petrology*. Prentice Hall, New Jersey, U.S.A.

Piper, J.D.A., Thomas, D.N., Share, S. and Zhang Qi Rui (1999) The palaeomagnetism of (Mesoproterozoic) Eriksfjord Group red beds, South Greenland: multiphase remagnetization during the Gardar and Grenville episodes. *Geophysical Journal International*, **136**, 739–756.

Poulsen, V. (1964) The sandstones of the Precambrian Eriksfjord Formation in South Greenland. *Rapport Grønlands Geologiske Undersøgelse*, **2**, 16 pp.

Price, R.C., Gray, C.M., Wilson, R.E., Frey, F.A. and Taylor, S.R. (1991) The effects of weathering on rare-earth element, Y and Ba abundances in Tertiary basalts from southeastern Australia. *Chemical Geology*, **93**, 245–265.

Ranløv, J. and Dymek, R.F. (1991) Compositional zoning in hydrothermal aegirine from fenites in the Proterozoic Gardar Province, South Greenland. *European Journal of Mineralogy*, **3**, 837–853.

Reiners, P.W., Nelson, B.K. and Ghiorso, M.S. (1995) Assimilation of felsic crust by basaltic magma: thermal limits and extents of crustal contamination of mantle-derived magmas. *Geology*, **23**, 563–566.

Roddick, J.C., Sullivan, R.W. and Dudas, F.Ö. (1992) Precise calibration of Nd tracer isotopic composition for Sm-Nd studies. *Chemical Geology*, **97**, 1–8.

Rollinson, H. (1993) *Using Geochemical Data: Evaluation, Presentation, Interpretation*. Longman Group UK, Limited, London.

Rudnick, R. and Fountain, D.M. (1995) Nature and composition of the continental crust: A lower crustal perspective. *Reviews of Geophysics*, **33**, 267–309.

Rumble, D. and Hoering, T.C. (1994) Analysis of oxygen and sulfur isotope ratios in oxide and sulfide minerals by spot heating with a carbon dioxide laser in a fluorine atmosphrere. *Accounts of Chemical Research*, **27**, 237–241.

Schleicher, H., Kramm, U., Pernicka, E., Schidlowski, M., Schmidt, F., Subramanian, V., Todt, W. and Viladkar, S.G. (1998) Enriched subcontinental upper mantle beneath Southern India: Evidence from Pb,

Nd, Sr and C-O isotopic studies on Tamil Nadu carbonatites. *Journal of Petrology,* **39**, 1765–1785.

Sharp, Z.D. (1990) A laser-based microanalytical method for the in-situ determination of oxygen isotope ratios of silicates and oxides. *Geochimica et Cosmochimica Acta*, **54**, 1353–1357.

Shirey, S.B., Klewin, K.W., Berg, J.H. and Carlson, R.W. (1994) Temporal changes in the sources of flood basalts: Isotopic and trace element evidence from the 1100 Ma old Keweenawan Mamainse Point Formation, Ontario, Canada. *Geochimica et Cosmochimica Acta*, **58**, 4475–4490.

Simonetti, A., Goldstein, S.L., Schmidberger, S.S. and Viladkar, S.G. (1998) Geochemical and Nd, Pb, and Sr isotope data from Deccan alkaline complexes – inferences for mantle sources and plume-lithosphere interaction. *Journal of Petrology*, **39**, 1847–1864.

Steiger, R.H. and Jäger, E. (1977) Subcommision on geochronology: conventions of the use of decay constants in geo- and cosmochronology. *Earth and Planetary Science Letters*, **36**, 359–362.

Sun, S.S. and McDonough, W.F. (1989) Chemical and isotopic systematics of oceanic basalts: implications for mantle composition and processes. Pp. 313–345 in: *Magmatism in Ocean Basins* (A.D. Saunders and M.J. Norry, editors). Special Publication, **42**. Geological Society of London.

Taylor, P.N. and Upton, B.G.J. (1993) Contrasting Pb isotopic compositions in two intrusive complexes of the Gardar Magmatic Province of South Greenland. *Chemical Geology*, **104**, 261–268.

Taylor, P.N., Jones, N.W. and Moorbath, S. (1984) Isotopic assessment of relative contributions from crust and mantle sources to the magma genesis of Precambrian granitoid rocks. *Philosophical Transactions of the Royal Society of London*, **A310**, 605–625.

Taylor, S.R. and McLennan, S.M. (1985) *The Continental Crust: its Composition and Evolution*. Blackwell Scientific Publications, Oxford, UK.

Thomas, D.N. and Piper, J.D.A. (1992) A revised magnetostratigraphy for the Mid-Proterozoic Gardar lava succession, South Greenland. *Tectonophysics*, **201**, 1–16.

Turner, S.P., Hawkesworth, C.J., Gallagher, K.G., Stewart, K., Peate, D. and Mantovani, M. (1996) Mantle plumes, flood basalts and thermal models for melt generation beneath continents: assessment of a conductive heating model. *Journal of Geophysical Research*, **101**, 11503–11518.

Upton, B.G.J. (1996) Anorthosites and troctolites of the Gardar Magmatic Province. Pp. 19–34 in: *Petrology and Geochemistry of Magmatic Suites of Rocks in the Continental and Oceanic Crusts* (D. Demaiffe, editor). A volume dedicated to Professor Jean Michot, Université Libre de Bruxelles, Royal Museum for Central Africa (Tervuren).

Upton, B.G.J. and Emeleus, C.H. (1987) Mid-Proterozoic alkaline magmatism in southern Greenland: the Gardar province. Pp. 449–471 in: *The Alkaline Rocks* (J.G. Fitton and B.G.J. Upton, editors). Special Publication, **30**. Geological Society of London.

Upton, B.G.J., Emeleus, C.H., Heaman, L.M., Goodenough, K.M and Finch, A.A. (2003) Magmatism of the mid-Proterozoic Gardar Province, South Greenland: chronology, petrogenesis and geological setting. *Lithos*, **68**, 43–65.

Valley, J.W., Kitchen, N., Kohn, M.J., Niendorf, C.R. and Spicuzza, M.J. (1995) UWG-2, a garnet standard for oxygen isotope ratios: strategies for high precision and accuracy with laser heating. *Geochimica et Cosmochimica Acta*, **59**, 5223–5231.

van Breemen, O., Aftalion, M. and Allaart, J.H. (1974) Isotopic and geochronologic studies on granites from the Ketilidian Mobile Belt of South Greenland. *Bulletin of the Geological Society of America*, **85**, 403–412.

Vroon, P.Z., Lowry, D., Van Bergen, M.J., Boyce, A.J. and Mattey, D.P. (2001) Oxygen isotope systematics of the Banda Arc: Low $\delta^{18}O$ despite involvement of subducted continental material in magma genesis. *Geochimica et Cosmochimica Acta*, **65**, 589–609.

Waight, T., Baker, J. and Willigers, B. (2002) Rb isotope dilution analyses by MC-ICPMS using Zr to correct for mass fractionation: towards improved Rb-Sr geochronology? *Chemical Geology*, **186**, 99–116.

Walsh, J.N., Buckley, F. and Barker, J. (1981) The simultaneous determination of the rare-earth elements in rocks using Inductively Coupled Plasma Source Spectrometry. *Chemical Geology*, **33**, 141–153.

Weaver, B.L. (1991) The origin of ocean island basalt end-member compositions: trace element and isotopic constraints. *Earth and Planetary Science Letters*, **104**, 381–397.

Weaver, B.L., Wood, D.A., Tarney, J. and Joron, J.-L. (1987) Geochemistry of ocean island basalts from the South Atlantic: Ascension, Bouvet, St. Helena, Gough and Tristan da Cunha. Pp. 253–267 in: *The Alkaline Rocks* (J.G. Fitton and B.G.J. Upton, editors). Special Publication, **30**. Geological Society of London.

Winchester, J.A. and Floyd, P.A. (1976) Geochemical magma type discrimination; application to altered and metamorphosed basic igneous rocks. *Earth and Planetary Science Letters*, **28**, 459–469.

Zindler, A. and Hart, S.R. (1986) Chemical geodynamics. *Annual Reviews of Earth and Planetary Sciences*, **14**, 493–571.

[*Manuscript received 27 November 2002: revised 12 June 2003*]